Braz J Phys (2015) 45:457–466
DOI 10.1007/s13538-015-0332-0

SOCIEDADE BRASILEIRA DE FÍSICA

NUCLEAR PHYSICS

Hydrodynamic Simulations of the Combustion of Dense Hadronic Matter into Quark Matter

Marcos A. Albarracin Manrique[1] · **Germán Lugones**[2]

Received: 2 February 2015 / Published online: 12 May 2015

Abstract We perform special-relativistic one-dimensional hydrodynamic simulations to study the combustion of hadronic matter into quark matter in neutron star conditions. For the equation of state, we use a relativistic mean-field Walecka model for hadronic matter and the MIT bag model for quark matter. We study the growth of a small core of quark matter surrounded by hadronic matter at constant density, where both regions are initially at rest. We show that a strong detonation front propagates into hadronic matter converting it into quark matter. We find that the timescale for the conversion of a compact star is around tens of microseconds.

Keywords Neutron star · Hydrodynamics

1 Introduction

Observational evidence is not conclusive about the internal composition of compact stars. All measured stellar properties such as masses, radii, cooling properties, pulsar frequencies, etc. are compatible at present with a pure hadronic composition, but also with models that allow the presence of deconfined quark matter (hybrid or strange quark stars) [1]. In fact, the core of compact stars can reach densities that are several times larger than the saturation density of nuclear matter. In such extreme conditions strongly interacting matter may undergo a phase transition from confined hadronic matter to quark matter. The formation of quark matter in a compact star is expected to begin with the nucleation of small deconfined drops inside the stellar core when the density of hadronic matter goes beyond a critical density [2–10, 13]. Such critical density can be reached if a cold hadronic star gains mass due to accretion in a binary system. Another possibility is related to the loss of rotational energy due to the emission of gravitational waves which leads to a contraction of the star. It is also possible that a protoneutron star at the center of a supernova explosion gains large amounts of matter due to fallback accretion. If the explosion energy is not large enough, the inner part of the progenitor star falls back onto the central remnant and only the outer part of the star overcomes the gravitational potential. Other possible mechanisms are the merging of compact objects, and strangelet contamination if quark matter is absolutely stable.

According to recent studies [2–10, 13], the quark matter deconfinement occurs in two steps. First, hadrons composing nuclear matter deconfine in a strong interaction time scale of $\sim 10^{-23}$ seconds to quark matter, leaving a quark gas which is not in equilibrium under weak interactions. Later, weak interactions will chemically equilibrate the system in a time scale of $\sim 10^{-8}$ s. As a result of these weak decays, temperature is significantly increased, and a great amount of neutrinos is produced. The energy released in such conversion can ignite hadronic matter in the neighborhood of the drop, and as a consequence, it may grow and convert to quark matter the core of the star

✉ Germán Lugones
german.lugones@ufabc.edu.br

Marcos A. Albarracin Manrique
sagret10@usp.br

[1] Instituto de Física, Universidade de São Paulo, Rua do Matão Travessa R Nr. 187, CEP 05508-090 Cidade Universitária, São Paulo, Brazil

[2] Centro de Ciências Naturais e Humanas, Universidade Federal do ABC, Rua Santa Adélia, 166, 09210-170, Santo André, Brazil

and even the whole star if quark matter is absolutely stable. During the conversion, a combustion front (flame) separating the unburnt hadronic matter from the burnt quark matter travels outwards along the star [15–25].

The front of the flame propagates with a velocity of the order of $c/\sqrt{3}$, where c is the speed of light [17]. At the flame front, there is a region of thickness $l_{strong} = \tau_{strong} \times c/\sqrt{3} = 10^{-23}\text{s} \times c/\sqrt{3} \sim 1\text{fm}$ where hadronic matter deconfines. Behind it, there is a region of thickness $l_{weak} = \tau_{weak} \times c/\sqrt{3} = 10^{-8}\text{s} \times c/\sqrt{3} \sim 1\text{m}$ where quark matter reaches chemical equilibrium through weak interactions. This order of magnitude estimates shows that the flame is very thin compared with the size of the star (~ 10 km). For this reason, it is a good approximation to treat the flame as a mere surface of discontinuity between the burnt and unburnt fluids.

The objective of our work is to study the hydrodynamic propagation of the flame by means of one-dimensional relativistic hydrodynamic simulations employing realistic equations of state (EOS) for both the hadronic and the quark matter phase. More specifically, we want to determine the propagation speed of the combustion and the time it would take a hadronic star to be converted into a hybrid or a strange star.

2 Relativistic Hydrodynamic Equations and Numerical Method

For studying the propagation of the combustion process of hadronic matter into quark matter inside neutron stars, we consider the relativistic one-dimensional time-dependent Euler equations within the frame of special relativity. In such a case, the compressible Euler equations form a system of three equations [26, 27],

$$\begin{aligned} (u^\alpha \rho)_{,\alpha} &= 0, \\ T^{\alpha\beta}_{\ ,\alpha} &= 0 \quad \text{with} \quad \beta = 0, 1, \end{aligned} \tag{1}$$

where "$,\alpha$" denotes partial differentiation with respect to the coordinate x^α, and $T^{\alpha\beta}$ is the stress energy tensor for a perfect fluid

$$T^{\alpha\beta} = \rho h u^\alpha u^\beta + p\eta^{\alpha\beta}. \tag{2}$$

Here, u^α are the components of the 2-velocity, ρ is the proper mass density, p is the pressure, e is the specific internal energy, $h = 1 + e + p/\rho$ is the total specific enthalpy, and $\eta^{\alpha\beta}$ is the Minkowski metric tensor. For convenience, we use units where the speed of light is $c = 1$.

The special relativistic Euler equations can be written as a system of conservation laws [28]:

$$\mathbf{U}_t + \mathbf{F}(\mathbf{U})_x = 0, \tag{3}$$

where in the laboratory frame the *state vector* $\mathbf{U}$ contains the *conserved* variables (D, S, τ) written in terms of *primitive* variables (ρ, v, p)

$$\mathbf{U} = \begin{bmatrix} D \\ S \\ \tau \end{bmatrix} = \begin{bmatrix} \gamma_l \rho \\ \rho h \gamma_l^2 v \\ \rho h \gamma_l^2 - p - \gamma_l \rho \end{bmatrix}, \tag{4}$$

and the *flux vector* $\mathbf{F}$ is given by

$$\mathbf{F} = \begin{bmatrix} Dv \\ Sv + p \\ S - Dv \end{bmatrix}, \tag{5}$$

with $\gamma_l = (1 - v^2)^{-1/2}$ being the Lorentz factor. The elements of the flux matrix are the mass flux Dv, the momentum flux plus pressure force $Sv + p$, and the energy flux plus pressure work $\tau v + pv = S - Dv$. Note that the flux vector must be expressed in terms of the conserved variables of the state vector. Additionally, an equation of state relating the thermodynamic variables is needed to close the system, which we assume to be given in the form $e = e(p, \rho)$.

The conservation laws presented above can be numerically solved through several methods. In the present work, we shall employ a *High-Resolution Shock-Capturing* scheme which is recognized as a very efficient scheme for dealing with complex flows specially when discontinuities are present (see, e.g., Ref. [1] for more details). These methods use the equations in conservative form together with approximate or exact Riemann solvers to calculate the numerical fluxes between neighboring computational cells. This fact guarantees the capture of all discontinuities (e.g., shock waves) which naturally appear in spatial solutions of the nonlinear hyperbolic equations and allows high accuracy in regions where the fluid flow is smooth. These schemes depend on the spectral decomposition of the Jacobian matrix $\partial\mathbf{F}/\partial\mathbf{U}$ which has a complete set of linearly independent eigenvectors (characteristic fields) $\mathbf{K}_i$, and corresponding eigenvalues (characteristic velocities) such that

$$\left[\frac{\partial \mathbf{F}}{\partial \mathbf{U}}\right] \mathbf{K}_i = \lambda_i \mathbf{K}_i, \qquad i = 1, 2, 3. \tag{6}$$

In the one dimensional case, the eigenvalues and eigenvectors are given by [30–32]

$$\lambda_1 = \frac{v_x - c_s}{1 - v_x c_s}, \quad \lambda_2 = v_x, \quad \lambda_3 = \frac{v_x + c_s}{1 + v_x c_s}, \tag{7}$$

$$\begin{aligned} \mathbf{K}_1 &= [1, h\gamma_l \wp_1 \lambda_1, h\gamma_l \wp_1 - 1]^T, \\ \mathbf{K}_2 &= [\frac{\Omega}{h\gamma_l}, v, 1 - \frac{\Omega}{h\gamma_l}]^T, \\ \mathbf{K}_3 &= [1, h\gamma_l \wp_3 \lambda_3, h\gamma_l \wp_3 - 1]^T, \end{aligned} \tag{8}$$

where

$$\Omega \equiv \frac{\tilde{\kappa}}{\tilde{\kappa} - c_s^2}, \quad \tilde{\kappa} = \frac{1}{\rho}\frac{\partial p}{\partial e}, \quad \wp_{1,3} \equiv \frac{1 - v^2}{1 - v\lambda_{1,3}}. \tag{9}$$

The relativistic speed of sound in the fluid c_s is given by [32]

$$c_s^2 = |\frac{\partial p}{\partial E}|_{\mathcal{S}} = \frac{1}{h}|\frac{\partial p}{\partial \rho}|_e + \frac{p}{h\rho^2}|\frac{\partial p}{\partial e}|_\rho, \tag{10}$$

where $\mathcal{S}$ is the entropy per particle and $E = \rho + \rho e$ is the total rest energy density.

Our numerical code is based on the Godunov method [33] and the numerical fluxes are obtained using the well-known Riemann solver of Roe [34, 35]

$$\mathbf{f}_{i+1/2} = \frac{1}{2}(\mathbf{f}_r + \mathbf{f}_l) - \frac{1}{2}\sum_{k=1}^{3}\tilde{\mathbf{K}}_k|\tilde{\lambda}_k|\Delta\tilde{\omega}_k, \tag{11}$$

which has the advantage that can be straightforwardly implemented for an arbitrary EOS. The numerical fluxes $\mathbf{f}_l$ and $\mathbf{f}_r$ are computed using respectively the primitive variables to the left and right of the $i + \frac{1}{2}$ interface. The eigenvalues and eigenvectors $\tilde{\lambda}_i$ and $\tilde{\mathbf{r}}_i$ that appear in (11) are obtained by (7) and (8) using the following weighted quantities:

$$\tilde{\rho} = \sqrt{\rho_l \rho_r}, \tag{12}$$

$$\tilde{v} = \frac{\sqrt{\rho_l}v_l + \sqrt{\rho_r}v_r}{\sqrt{\rho_l} + \sqrt{\rho_r}}, \tag{13}$$

$$\tilde{h} = \frac{\sqrt{\rho_l}h_l + \sqrt{\rho_r}h_r}{\sqrt{\rho_l} + \sqrt{\rho_r}}. \tag{14}$$

The quantities $\{\Delta\tilde{\omega}_k\}$ represent the jumps of the characteristic variables across each characteristic field and are obtained from the inversion of:

$$\Delta\mathbf{U} = \mathbf{U}_r - \mathbf{U}_l = \sum_{k=1}^{3}\Delta\tilde{\omega}_k\tilde{\mathbf{K}}_k. \tag{15}$$

To solve equations numerically, the system is discretized in space intervals Δx and time steps Δt of variable size; thus,

$$\mathbf{U}_i^{n+1} = \mathbf{U}_i^n + \frac{\Delta t}{\Delta x}[\mathbf{f}_{i-1/2} - \mathbf{f}_{i+1/2}], \tag{16}$$

where the intercell numerical flux is given by (11). The stability of the scheme requires that the solutions to the Riemann problems at the cell edges do not interact during the time step Δt. This is satisfied by imposing the Courant-Friedrichs and Lewy (CFL) condition [35] $\Delta t \leq C_{cfl}\Delta x/S_{max}^n$, where C_{cfl} is the Courant number satisfying $0 < C_{cfl} \leq 1$ and S_{max}^n is the largest wave speed present throughout the domain at time level n. In this work, we consider $C_{cfl} = 0.9$ and $S_{max}^n = \max[(u + c)/(1 + uc), (u - c)/(1 - uc)]$ to calculate the maximum wave velocity.

3 Equations of State

The true EOS that describes the interior of compact stars is still uncertain at very high densities, due to our inability to test matter experimentally beyond twice the nuclear density and the severe computational difficulties that arise when trying to solve the equations of QCD in the non-perturbative regime. In view of this, many different phenomenological EOSs have been proposed that satisfy the currently available observational constraints. In this work, we use a relativistic mean-field (Walecka) model for hadronic matter and the MIT bag model for quark matter, both of which are widely used to describe hadronic matter in compact stars.

3.1 The Walecka Model

For the hadronic phase, we use a nonlinear Walecka model [36–39] including the whole baryon octet, electrons, and the corresponding antiparticles. The Lagrangian is given by

$$\mathcal{L} = \mathcal{L}_B + \mathcal{L}_M + \mathcal{L}_L, \tag{17}$$

where the indices B, M, and L refer to baryons, mesons, and leptons, respectively. For the baryons, we have

$$\mathcal{L}_B = \sum_B \bar{\psi}_B\left[\gamma^\mu\left(i\partial_\mu - g_{\omega B}\,\omega_\mu - g_{\rho B}\,\vec{\tau}\cdot\vec{\rho}_\mu\right) - (m_B - g_{\sigma B}\,\sigma)\right]\psi_B, \tag{18}$$

with B extending over nucleons n, p and the following hyperons Λ, Σ^+, Σ^0, Σ^-, Ξ^-, and Ξ^0. The contribution of the mesons σ, ω, and ρ is given by

$$\mathcal{L}_M = \frac{1}{2}(\partial_\mu\sigma\,\partial^\mu\sigma - m_\sigma^2\sigma^2) - \frac{b}{3}m_N(g_\sigma\sigma)^3 - \frac{c}{4}(g_\sigma\sigma)^4 - \frac{1}{4}\omega_{\mu\nu}\,\omega^{\mu\nu} + \frac{1}{2}m_\omega^2\,\omega_\mu\,\omega^\mu - \frac{1}{4}\vec{\rho}_{\mu\nu}\cdot\vec{\rho}^{\mu\nu} + \frac{1}{2}m_\rho^2\,\vec{\rho}_\mu\cdot\vec{\rho}^\mu, \tag{19}$$

and the coupling constants are

$$g_{\sigma B} = x_{\sigma B}g_\sigma,\ g_{\omega B} = x_{\omega B}g_\omega,\ g_{\rho B} = x_{\rho B}g_\rho. \tag{20}$$

Electrons are included as a free Fermi gas, $\mathcal{L}_L = \sum_l \bar{\psi}_l\,(i\partial\!\!\!/ - m_l)\,\psi_l$, in chemical equilibrium with all other particles.

The constants in the model are determined by the properties of nuclear matter and hyperon potential depths known from hypernuclear experiments. In the present work, we use the GM1 parametrization for which we have $(g_\sigma/m_\sigma)^2 = 11.79\ \text{fm}^{-2}$, $(g_\omega/m_\omega)^2 = 7.149\ \text{fm}^{-2}$, $(g_\rho/m_\rho)^2 = 4.411\ \text{fm}^{-2}$, $b = 0.002947$ and $c = 0.001070$ [39]. For the hyperon coupling constants, we adopt $x_{\sigma i} = x_{\rho i} = 0.6$ and $x_{\omega i} = 0.653$ [39]. For details on the explicit form of the

equation of state derived from this Lagrangian, the reader is referred to Ref. [10].

Notice that the maximum mass configuration of non-rotating stars for the here-used hadronic EOS is below two solar masses and therefore conflicts with the discovery of the pulsars PSR J1614-2230 with $M = (1.97 \pm 0.04)M_{\odot}$ [40] and PSR J0348-0432 with $M = (2.01 \pm 0.04)M_{\odot}$ [41]. In future work, we will improve this using more realistic parametrizations. However, as we discuss below, the employed parametrization has not major effects within the present hydrodynamic model.

3.2 The MIT bag Model

We describe the quark phase as a non-interacting charge-neutral gas composed by massless u, d, and s quarks and their antiparticles. Notice that, since strange quarks are considered to be massless, no leptons are necessary to achieve electric charge neutrality. Under such assumptions, all quarks can be described by only one chemical potential and the EOS within the MIT bag model reads:

$$\begin{aligned} P &= \frac{19}{36}\pi^2 T^4 + \frac{3}{2}T^2\mu^2 + \frac{3}{4\pi^2}\mu^4 - B, \\ E &= \frac{19}{12}\pi^2 T^4 + \frac{9}{2}T^2\mu^2 + \frac{9}{4\pi^2}\mu^4 + B, \\ n_B &= T^2\mu + \frac{1}{\pi^2}\mu^3, \end{aligned} \tag{21}$$

where P is the pressure, E the total energy density and n_B the baryon number density (see Ref. [13] and references therein). Since the quark's masses and the strong coupling constant were set to zero, the only parameter in this model is the bag constant B. According to the above equations, the pressure is related to the energy density through

$$P = \frac{1}{3}(E - 4B). \tag{22}$$

Using a finite s-quark mass would be more realistic, but in this case an analytic expression for the equation of state is no longer possible for finite temperatures. The EOS would involve Fermi integrals that are computationally time costly in a hydrodynamic code. However, as we discuss below, the use of massless quarks is not a bad approximation within our hydrodynamic model because the deconfinement density is not very sensitive to the strangeness fraction.

Stars containing quark phases can be hybrid stars (where quark matter is restricted to the core) or strange stars (made up completely by quark matter), depending on whether the energy per baryon of quark matter in equilibrium under weak interactions is less than the neutron mass at zero pressure and zero temperature. If the energy per baryon of quark matter at $P = T = 0$ is less than the neutron mass, the true and absolute ground state of strongly interacting matter is a deconfined state of quark matter consisting of an approximately equal proportion of up, down, and strange quarks. In such a case, quark matter is said to be absolutely stable and it is referred to as *strange matter*. In fact, Farhi and Jaffe [42] found that quark matter in bulk can be absolutely stable if the bag constant falls in the range 57 MeV fm^{-3} $< B <$ 92 MeV fm^{-3}. In this work, we employ B = 80 MeV/fm^3 corresponding to strange matter and B = 120 MeV /fm^3 corresponding to quark matter that is allowed only at high pressures.

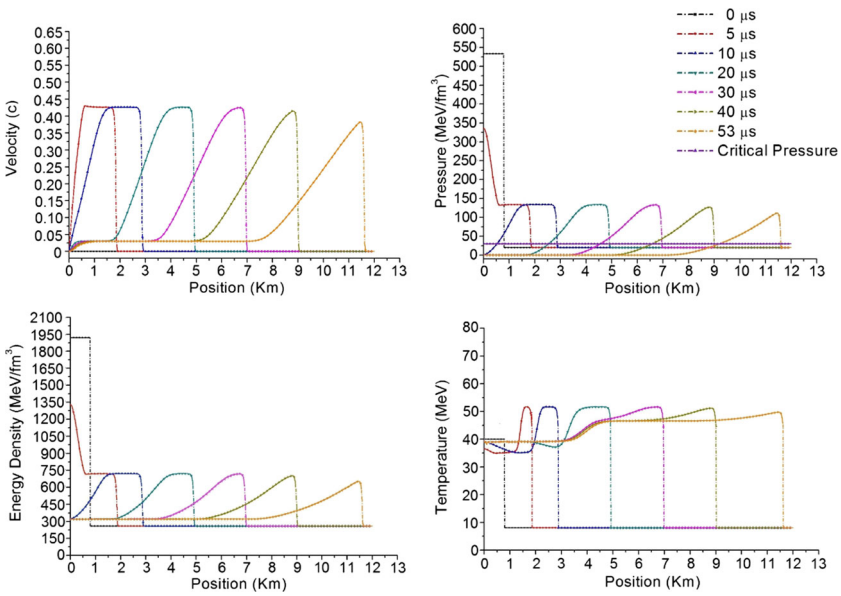

Fig. 1 Velocity, pressure, energy density, and temperature profiles for different times (in microseconds). The bag constant is 80 MeV/fm^3. The initial pressures are $P_{in}^q = 533$ MeV/fm^3 and $P_{in}^h = 20$ MeV/fm^3 and the initial temperatures are $T_q = 40$ MeV and $T_h = 8$ MeV. Notice that a detonation wave is formed almost instantaneously due to the large gradients in the initial profile. The detonation wave has a velocity of the order of $\sim 0.4c$ and reaches the "surface of the star" in approximately 53 μs

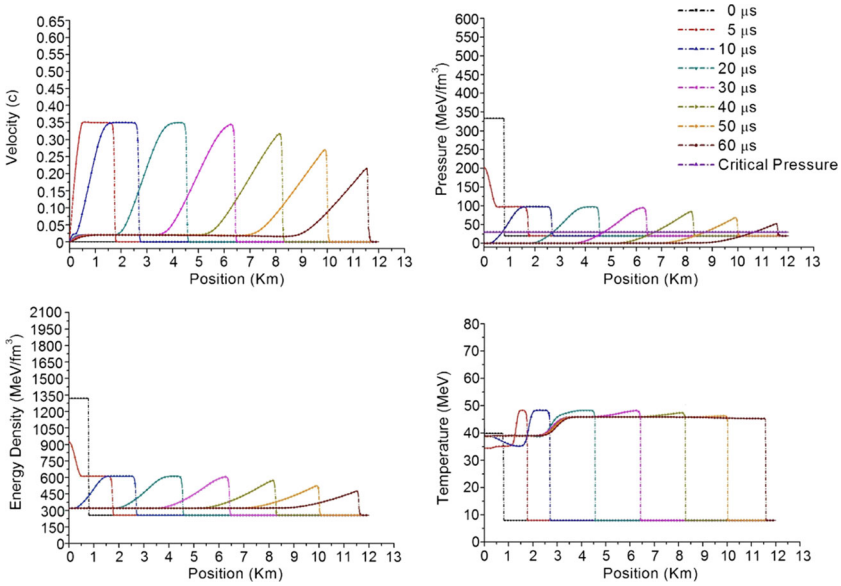

Fig. 2 Same as Fig. 1 (i.e., $B = 80\ \mathrm{MeV/fm^3}$) but for initial pressures $P_{in}^{q} = 333\ \mathrm{MeV/fm^3}$ and $P_{in}^{h} = 20\ \mathrm{MeV/fm^3}$. As in the previous figure, a detonation wave is formed almost instantaneously which crosses the system in $\sim 60\mu s$

4 Numerical Simulations

4.1 Description of the Model

Boundary conditions In order to mimic the boundary conditions in a neutron star, we have considered a one-dimensional computational domain with a closed end (i.e., reflective boundary conditions) which would correspond to the center of the star, and an open end (i.e., transmissive boundary conditions) that would correspond to the surface of the star. We study the hydrodynamic evolution of a small core of quark matter surrounded by hadronic matter, where both regions are initially at rest.

Deconfinement criterium An important aspect in the numerical simulation is the implementation of a criterium for the onset of the deconfinement transition.

In this work, we shall assume that hadronic matter deconfines if it has a pressure larger than a critical value P_{crit}. The critical pressure is determined by the Gibbs' criterion, i.e., equality of pressure P, temperature T, and Gibbs free energy per baryon g in both phases [2–10, 13]: $T^h = T^q$, $P^h = P^q$, $g^h = g^q$. On the other hand, deconfinement is driven by strong interactions and therefore quark flavor must be conserved during the deconfinement transition [2–10, 13]. This means that the abundances of all particle species in just deconfined quark matter must be *initially*

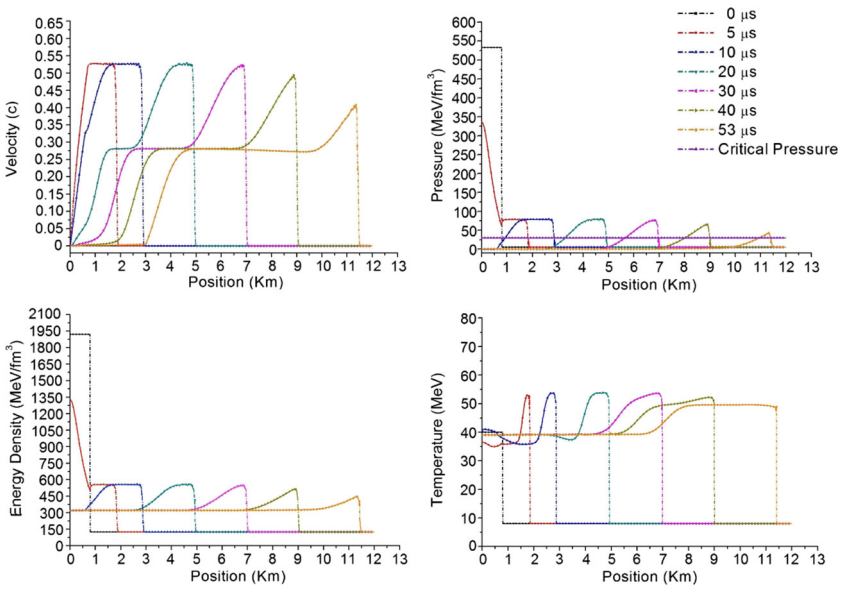

Fig. 3 Same as Fig. 1 (i.e., $B = 80\ \mathrm{MeV/fm^3}$) but for $P_{in}^{q} = 533\ \mathrm{MeV/fm^3}$ and $P_{in}^{h} = 5\ \mathrm{MeV/fm^3}$. Initially, the detonation front has a larger velocity than in Figs. 1 and 2 due to the larger ΔP in the initial condition

the same as in the hadronic matter from which it has been originated. Thus, we have $Y_f^h = Y_f^q$, with $f = u, d, s, e$, being $Y_f^h \equiv n_f^h/n_B^h$ and $Y_i^q \equiv n_f^q/n_B^q$ the abundances of each particle species in the hadron and quark phase, respectively. The calculation of the critical pressure has been done in Ref. [15] and the corresponding values are $P_{crit} = 30$ MeV/fm^3 for $B = 80$ MeV/fm^3 and $P_{crit} = 90$ MeV/fm^3 for $B = 120$ MeV/fm^3. Since the critical pressure depends on the mass of the strange quark m_s, we adopted P_{crit} corresponding to $m_s = 100$ MeV, which gives a more realistic value.

Notice that just deconfined matter is transitorily out of equilibrium under weak interactions. After some time (typically $\tau_{weak} \sim 10^{-8}$ s), weak interactions drive it to a β-stable configuration. During the process of β-equilibration, there is an energy release that rises the temperature of quark matter to $\sim$ 40 MeV [43–48]. An inclusion of these weak decay processes in the hydrodynamic simulation is out of the scope of the present work since it involves the solution of the Boltzmann equation with the appropriate decay rates for all the fluid elements within the flame. Therefore, as a first step towards a complete hydrodynamic simulation of the combustion process, we shall use the following approximate procedure: If hadronic matter achieves the critical pressure P_{crit}, the composition of that piece of fluid is instantaneously changed to β-stable quark matter with the same pressure and the same baryon number density.

Previous works on the hadron-quark combustion have employed different conditions for triggering the conversion in the hydrodynamic simulations. In Ref. [22], it is assumed that deconfinement is triggered by the diffusion of strange quarks from the burnt fluid (strange quark matter) to the flame front. This assumption about the microphysical mechanism of combustion process leads to slow propagation speeds for the flame front. In our work, deconfinement is triggered directly by the hydrodynamic compression of the flame front, provided that matter attains the critical pressure. Of course, both mechanisms can operate in a realistic flame, but the one considered in our work is dominant (if present) and leads to much faster propagation speeds. On the other hand, the condition used in Refs. [23, 25] is the requirement that combustion must be exothermic. Such condition, already employed in Ref. [17], is a necessary but not sufficient condition for combustion. It relates the state of unburnt hadronic matter with fully burnt quark matter behind the flame. The condition used in our work relates unburnt hadronic matter with just deconfined matter that is still out of equilibrium under weak interactions and is a sufficient condition for the burning to begin. Notice that the strange fraction in quark matter is not a key ingredient in our simulations because deconfinement is not triggered by strange quark diffusion as in Ref. [22], but by direct hydrodynamic compression of the fluid.

Initial conditions For simplicity, we shall begin our simulations at a stage where the initial drop of deconfined quarks has grown to form a small macroscopic stellar core. In all cases, the size of the initial core of quark matter is considered to be 800 m, and the rest of the computational domain (with length $R = 12$ km) is occupied by hadronic matter. Both regions are initially at rest. Notice that we are not including the effect of gravity in our hydrodynamic simulations, and therefore hadronic matter has been put at constant density in order to avoid a spurious motion of the unburnt

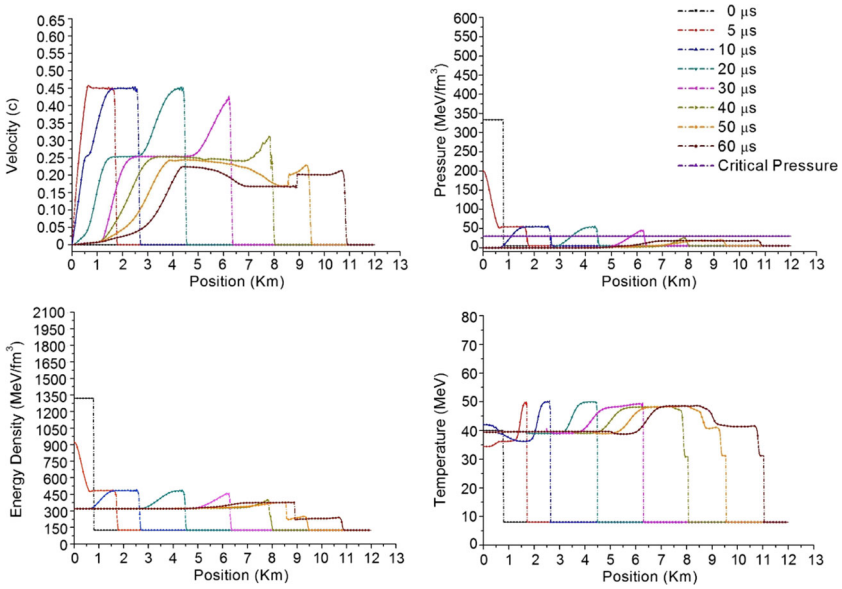

Fig. 4 Same as Fig. 1 (i.e. $B = 80$ MeV/fm^3) but for $P_{in}^q = 333$ MeV/fm^3 and $P_{in}^h = 5$ MeV/fm^3. A detonation front is formed but it decelerates significantly as it goes through hadronic matter. In the plot for the pressure we notice that for $t \sim 40\mu s$ the pressure at the flame is smaller than the critical pressure meaning that the flame turns-off and propagates through hadronic matter as a shock wave without producing any phase conversion

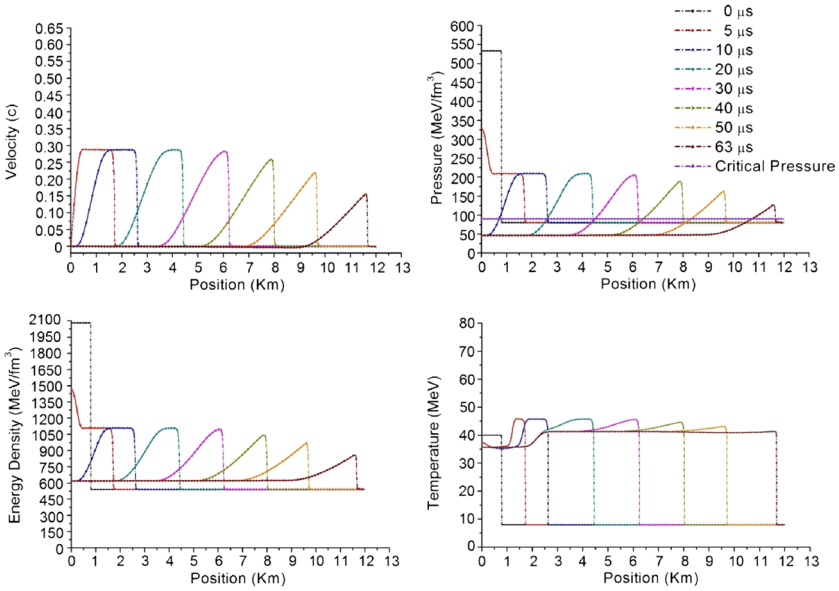

Fig. 5 Same as previous figures but for a bag constant $B = 120$ MeV/fm^3. The initial pressures are $P_{in}^q = 533$ MeV/fm^3 and $P_{in}^h = 80$ MeV/fm^3. As in previous figures, a detonation wave is formed almost instantaneously with a velocity of the order of $\sim 0.3c$. Again, the combustion advances through hadronic matter and it is gradually decelerated. It reaches the "surface of the star" in approximately 63 μs with a velocity of the order of $\sim 0.15c$

fluid before the passage of the combustion front. As a consequence, our calculations are not sensitive to the different density variations arising from different parametrizations of the EOS. The strangeness content of matter depends on the parametrization but as discussed above it is not essential within the present model because deconfinement is not triggered by strange quark diffusion as in Ref. [22].

As explained before, we employ the GM1 parametrization of the Walecka model EOS for hadronic matter and two different parameterizations of the MIT bag model EOS for quark matter, with $B = 80$ and 120 MeV/fm^3. In the case with $B = 80$ MeV/fm^3, we adopt two different values for the initial pressure of the quark core: $P_{in}^q = 533$ MeV/fm^3 and $P_{in}^q = 333$ MeV/fm^3 which correspond respectively to $\sim$ 13 and 9 times the nuclear saturation density. For the hadronic phase, we adopt $P_{in}^h = 20$ MeV/fm^3 and $P_{in}^h = 5$ MeV/fm^3 which correspond respectively to ~ 2 and 1 times the nuclear saturation density. In the case with $B = 120$ MeV/fm^3, we use $P_{in}^q = 533$ MeV/fm^3 and $P_{in}^q = 333$ MeV/fm^3 for quark matter. For the hadronic phase, we adopt $P_{in}^h = 80$ MeV/fm^3 and $P_{in}^h = 50$ MeV/fm^3 which correspond respectively to $\sim$ 3.3 and 2.8 times the nuclear saturation density. In all cases, the initial temperatures are $T^h = 8$ MeV and $T^q = 40$ MeV.

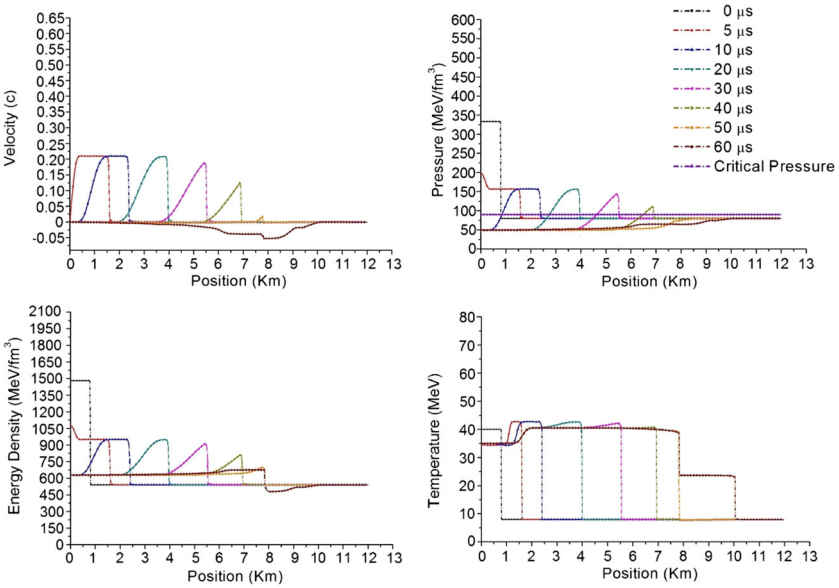

Fig. 6 Same as Fig. 5 (i.e., $B = 120$ MeV/fm^3) but for $P_{in}^q = 333$ MeV/fm^3 and $P_{in}^h = 80$ MeV/fm^3. Notice that the flame turns-off at $t \sim 50\mu s$. Since the pressure behind the flame is smaller that ahead it, the fluid begins to move downwards (negative velocity)

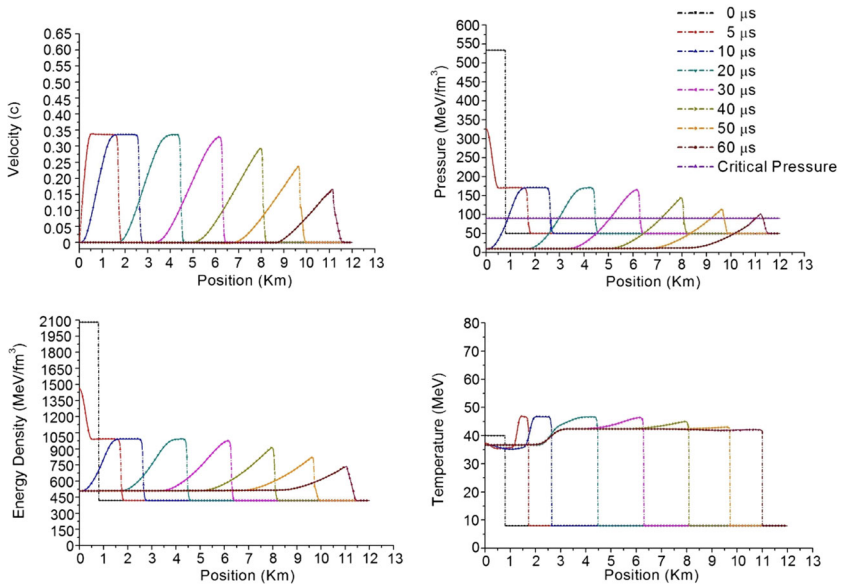

Fig. 7 Same as Fig. 5 (i.e., $B = 120$ MeV/fm^3) but for $P_{in}^q = 533$ MeV/fm^3 and $P_{in}^h = 50$ MeV/fm^3

4.2 Results

In Figs. 4, 5, 6, 7, 8, we show the velocity, pressure, energy density, and temperature profiles at different times for several initial conditions. In Figs. 1, 2, 3, 4, the results are shown for $B = 80$ MeV/fm^3 and in Fig. 5–8 for $B = 120$ MeV/fm^3. Notice that in all the simulations, a detonation wave is formed almost instantaneously and is followed by a rarefaction wave in coincidence with what it is known from the literature [17, 49]. We have explored several initial conditions (not shown here), and we have never found the formation of a deflagration front. We find that the detonation wave has an initial velocity in the range $0.20-0.55c$ and in most cases it reaches the end of the computational domain in $t \sim 50-65\ \mu$s. In some cases, the flame is strongly decelerated and turns off before reaching the surface of the star. This happens when the initial pressure gradient between the burnt and unburnt regions is not too large. The temperature in the burnt region is $\sim 30-50$ MeV, in agreement with the previous calculations [17].

Notice that in some cases, the pressure in the burnt region may have values below the critical pressure. As explained before, quark matter is absolutely stable for $B = 80$ MeV/fm^3 and therefore quark matter does not convert back to hadronic matter even if $P < P_{crit}$. However, for $B = 120$ MeV/fm^3, quark matter is not absolutely stable and it should convert back to hadronic matter if $P < P_{crit}$. In spite of this, we have not allowed this back conversion to happen in

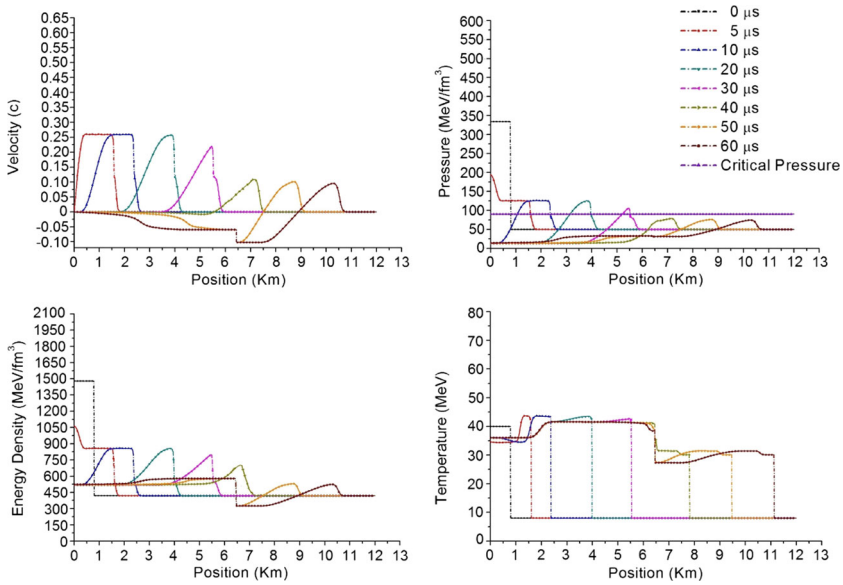

Fig. 8 Same as Fig. 5 (i.e., $B = 120$ MeV/fm^3) but for $P_{in}^q = 333$ MeV/fm^3 and $P_{in}^h = 50$ MeV/fm^3. As in Figs. 4 and 6 the flame turns-off in $\sim 40\mu s$

the simulations because we expect that in a more realistic situation gravity will compress burnt matter and maintain it above P_{crit} within the core of the neutron star.

We also find that in all simulations the combustion mode corresponds to the so called strong detonations having a supersonic motion with respect to the unburnt fluid and a subsonic velocity with respect to the burnt phase immediately behind the flame ($v_q < c_{sq}$, being c_{sq} the sound speed of quark matter).

5 Summary and Conclusions

In this work, we studied the combustion of hadronic matter into quark matter using a hydrodynamic 1D code to solve numerically the special-relativistic one-dimensional Euler equations. To describe the thermodynamic properties of dense matter in neutron star conditions, we employed standard equations of state for both the hadronic and the quark matter phase. In the case of quark matter, we employed two different parameterizations of the MIT bag model EOS: $B = 80$ MeV/fm^3 that corresponds to the Witten's hypothesis of absolute stability of quark matter and $B = 120$ MeV/fm^3 that corresponds to the more conservative case of quark matter that is not absolutely stable. For simplicity, our code does not include the effect of gravity. Thus, in order to mimic the boundary conditions in a neutron star, we have considered a computational domain with a closed end (i.e., reflective boundary conditions) which would correspond to the center of the star, and an open end (i.e., transmissive boundary conditions) that would correspond to the surface of the star.

As a criterium for the onset of the deconfinement transition, we assumed that hadronic matter deconfines if it has a pressure larger than a critical value P_{crit}. The critical pressure can be determined employing the flavor conservation condition together with the standard Gibbs' criterion, i.e., equality of pressure P, temperature T and Gibbs free energy per baryon g in both, the hadronic and the just deconfined phases. If during the simulation, a piece of hadronic matter achieves the critical pressure, the equation of state of that piece of fluid is instantaneously changed to quark matter.

The deconfinement transition inside a neutron star should begin with the nucleation of a microscopic drop of quark matter near the center of the star [2–10, 13]. For simplicity, we began our simulations at a stage where the initial drop has grown to a macroscopic size. In all the simulations, we considered initially a core of quark matter at rest with a size of 800 m and the rest of the computational domain (with size $R = 12$ km) is occupied by hadronic matter at rest. The results are not sensitive to the exact size of the central core. In the hydrodynamic simulations, we have explored several initial conditions for the pressure and the temperature of both phases. In all cases, we observe that a strong detonation wave is formed almost instantaneously. The flame front develops an initial velocity in the range $0.20 - -0.55c$ and crosses the whole computational domain in $t \sim 50 - -65\mu$s. We have never found the formation of a deflagration front. When the initial pressure gradient between the burnt and unburnt regions is not too large, we observe that the flame turns off before reaching the surface of the star and propagates through hadronic matter as a shock wave without producing any phase conversion. The temperature in the burnt region is $\sim$ 30–50 MeV, in coincidence with previous estimates [17].

There some recent works that have addressed the combustion of hadronic matter into quark matter. In Ref. [22], the authors numerically investigate the combustion of pure neutron matter to strange quark matter, taking into account binding energy release and neutrino emission across the burning front. In their model the combustion proceeds due to strange quark diffusion, which is a very slow mechanism to propagate the conversion. As a result, they find typical speeds of the burning process to be between 0.002 c and 0.04 c. In Refs. [23, 25] the authors present three-dimensional non-relativistic numerical simulations of turbulent combustion converting a neutron star into an absolutely stable strange quark star. In all cases they observe growing Rayleigh-Taylor instabilities of the conversion front. The resulting turbulent motion strongly enhances the conversion velocity but the burning speed does not reach sonic or even supersonic velocities. Despite assuming absolutely stable strange quark matter, a spherical SQM interior surrounded by an outer layer of hadronic matter is always formed at the end of the simulations. This outer layer exists because in their hydrodynamic approximation the combustion stops when the conversion front reaches conditions under which exothermic burning is no longer possible. Our work is complementary to these previous studies. Although we have not included several ingredients such as weak interaction decays, neutrino transport within the flame and gravity, we have considered some key ingredients that were not included in the previous works. One is the use relativistic hydrodynamic simulations. Notice that the calculations presented in Refs. [22, 23, 25] employ non-relativistic hydrodynamics. Additionally, our treatment of the deconfinement process is different to the adopted in Refs. [22, 23, 25].

In summary, our main result is the confirmation by relativistic hydrodynamic simulations that the conversion of a hadronic matter into a quark matter should proceed trough a detonation mode that would convert a compact star in a timescale of tens of microseconds. Certainly, a more realistic simulation should include the effect of gravity. Nevertheless, if gravity was included, the combustion process would be helped by the release of gravitational binding energy provided by the contraction of the quark matter

core. Moreover, the presence of gravity leads to the onset of hydrodynamic instabilities in the flame that enlarge the effective surface area available for ignition increasing the possibility of propagation in the form of a detonation. Thus, we don't expect that gravity would change significantly the here-found timescale for the conversion of the star.

Acknowledgments UFABC and CAPES are acknowledged for support. G.L. acknowledges the financial support of FAPESP and CNPq.

References

1. Buballa, et al., J. Phys. **123001**, G41 (2014)
2. M.L. Olesen, J. Madsen, Phys. Rev. **D49**, 2698 (1994)
3. G. Lugones, O. Benvenuto, Phys. Rev. **D58**, 083001 (1998)
4. K. Iida, K. Sato, Phys. Rev. **C58**, 2538 (1998)
5. O.G. Benvenuto, G. Lugones, MNRAS **304**, L25 (1999)
6. I. Bombaci, I. Parenti, I. Vidaña, Astrophys. J. **614**, 314 (2004)
7. G. Lugones, I. Bombaci, Phys. Rev. **D72**, 065021 (2005)
8. I. Bombaci, G. Lugones, I. Vidaña, Astron. Astrophys. **462**, 1017 (2007)
9. I. Bombaci, D. Logoteta, P.K. Panda, C. Providencia, I. Vidaña, Phys. Lett. **B680**, 448 (2009)
10. G. Lugones, A.G. Grunfeld, N.N. Scoccola, C. Villavicencio, Phys. Rev. **D80** (2009)
11. G. Lugones, T.A.S. Do Carmo, A.G. Grunfeld, N.N. Scoccola, Phys. Rev. **D81**, 85012 (2010)
12. G. Lugones, A.G. Grunfeld. Phys. Rev. **D84**, 85003 (2011)
13. T.A.S. Do Carmo, G. Lugones, Physica **A 392**, 6536 (2013)
14. T.A.S. Do Carmo, G. Lugones, A.G. Grunfeld, J. Phys. G: Nucl. Part. Phys. **40**, 035201 (2013)
15. J.E. Horvath, O.G. Benvenuto, Phys. Lett. **B213**, 516 (1988)
16. O.G. Benvenuto, J.E. Horvath, Phys. Rev. Lett. **63**, 716 (1989)
17. G. Lugones, O.G. Benvenuto, H. Vucetich, Phys. Rev. **D50**, 6100 (1994)
18. G. Lugones, C.R. Ghezzi, E.M. De Gouveia Dal Pino, J.E. Horvath, Astrophys. J. **581**, L101 (2002)
19. I. Tokareva, A. Nusser, V. Gurovich, V. Folomeev, Int. J. Mod. Phys. **D14**, 33 (2005)
20. I. Tokareva, A. Nusser, Phys. Lett. **B639**, 232 (2006)
21. P. Keranen, R. Ouyed, P. Jaikumar, Astrophys. J. **618**, 485 (2005)
22. B. Niebergal, R. Ouyed, P. Jaikumar, Phys. Rev. **C82**, 062801 (2010)
23. M. Herzog, F.K. Röpke, Phys. Rev. **D84**, 083002 (2011)
24. T. Fischer, et al., Astrophys. J. Supp. **194**, 39 (2011)
25. G. Pagliara, M. Herzog, F.K. Röpke, Phys. Rev. **D87**, 103007 (2013)
26. J. Smoller, B. Temple, Commun. Math. Phys. **156**, 67 (1993)
27. L.D. Landau, E.M. Lifshitz, *The Classical Theory of Fields Vol. 2* (Butterworth-Heinemann, 1975)
28. J.A. Font, T. Goodale, S. Iyer, M. Miller, L. Rezzolla, E. Seidel, N. Stergioulas, W.-M. Suen, M. Tobias, Phys. Rev. **D65**, 084024 (2002)
29. J.M. Martí, E. Müller, Living Rev. Relativ. **6**, 7 (2003)
30. J.A. Font, M. Miller, W.M. Suen, M. Tobias, Phys. Rev. **D61**, 044011 (2000)
31. F. Banyuls, J.A. Font, J.M. Ibañez, J.M. Marti, J.A. Miralles, Astrophys. J. **476**, 221 (1997)
32. O. Dönmez, Appl. Math. Comput. **181**, 256 (2006)
33. S.K. Godunov, Math. Sbornik. **47**, 271 (1959)
34. P.L. Roe, J. Pike, *Computing methods in applied science and engineering(INRIA North-Holland*, (Amsterdam, 1984)
35. E.F. Toro, *Riemann solvers and numerical methods for fluid dynamics: a practical introduction*, 3rd edn. (Springer-Verlag, Berlin, 2009)
36. J.D. Walecka, Ann. Phys. **83**, 491 (1974)
37. B.D. Serot, J.D. Walecka, Adv. Nucl. Phys. **16**, 1 (1986)
38. J. Boguta, R.A. Bodmer, Nucl. Phys. **A292**, 413 (1977)
39. N.K. Glendenning, S.A. Moszkowski, Phys. Rev. Lett. **67**, 2414 (1991)
40. P.B. Demorest, T. Pennucci, S.M. Ransom, M.S.E. Roberts, J.W.T. Hessels, Nature **467**, 1081 (2010)
41. J. Antoniadis, et al., Science **340**, 6131 (2013)
42. E. Farhi, R.L. Jaffe, Phys. Rev. **D30**, 2379 (1984)
43. J.D. Anand, A. Goyal, V.K. Gupta, S. Singh, Astrophys. J. **481**, 954 (1997)
44. L. Xiang-Jun, L. Zhi-Quan, L. Jing-Jing, L. Hong-Lin, Commun. Theor. Phys. **49**, 1643 (2008)
45. L. Xiang-Jun, L. Men-Quan, L. Jing-Jing, L. Zhi-Quan, Chin. Phys. **B17**, 585 (2008)
46. Zigao Dai, Q. Peng, T. Lu, Phys. Lett. **B319**, 199 (1993)
47. Z. Dai, Q. Peng, T. Lu, Astrophys. J. **440**, 815 (1995)
48. Z. Dai, X. Wu, T. Lu, Astrophys. Space Sci. **232**, 131 (1995)
49. L.D. Landau, E.M. Lifshitz, Vol. 6, *Fluid Mechanics* (Butterworth-Heinemann, 1987)